The formation of green rust induced by tropical river biofilm components

Frederic Jorand, Asfaw Zegeye, Jaafar Ghanbaja, Mustapha Abdelmoula

The formation of green rust induced by tropical river biofilm components

Running title: **Green rust from ferruginous biofilms**

Frédéric Jorand, Asfaw Zegeye, Jaafar Ghanbaja, Mustapha Abdelmoula

Abstract

In the Sinnamary Estuary (French Guiana), a dense red biofilm grows on flooded surfaces. In order to characterize the iron oxides in this biofilm and to establish the nature of secondary minerals formed after anaerobic incubation, we conducted solid analysis and performed batch incubations. Elemental analysis indicated a major amount of iron as inorganic compartment along with organic matter. Solid analysis showed the presence of two ferric oxides ferrihydrite and lepidocrocite. Bacteria were abundant and represented more than 10^{11} cells g^{-1} of dry weight among which iron reducers were revealed. Optical and electronic microscopy analysis revealed than the bacteria were in close vicinity of the iron oxides. After anaerobic incubations with exogenous electron donors, the biofilm's ferric material was reduced into green rust, a Fe^{II}-Fe^{III} layered double hydroxide. This green rust remained stable for several years. From this study and previous reports, we suggest that ferruginous biofilms should be considered as a favorable location for GR biomineralization when redox conditions and electron donors availability are gathered.

Keywords: green rust; biofilm; iron oxide; lepidocrocite; ferrihydrite; biomineralization; solid analysis; secondary iron minerals

1. INTRODUCTION

30

The green rust (GR) compounds are mixed Fe^{II}-Fe^{III} layered double hydroxide unstable under oxic conditions, and identified in several sub-oxic environments like corroded surface of Fe-based materials (Refait *et al.*, 2006), hydromorphic soils (Trolard *et al.*, 1997) or ground water (Christiansen *et al.*, 2009). The GR structure is

35   related to that of the mineral fougerite (IMA 2003-057) (Génin *et al.*, 2005; Trolard *et al.*, 2007). The GRs are considered to be key components in biogeochemical cycle of iron (Herbillon, 2006) or in the applied research for polluted soil and water remediation processes due to their high reactivity towards oxidized organic (nitroaromatics, chloride derived,…) or inorganic compounds (Hg^{II}, Se^{VI}, Cr^{VI},…)

40   (Myneni *et al.*, 1997; Erbs *et al.*, 1999; Loyaux-Lawniczak *et al.*, 2000; Refait *et al.*, 2000; O'Loughlin *et al.*, 2003). However, the mechanisms implied in their formation and whether or not bacteria are a major actor for their precipitation in natural environments, remain under investigation (Zegeye *et al.*, 2005 ; Zegeye *et al.*, 2007a ; Ahmed *et al.*, 2010 ; Salas *et al.*, 2010 ; Zegeye *et al.*, 2010).

45   The dissimilatory iron-reducing bacteria (DIRB) are well recognized to be involved in the formation of secondary iron-II minerals. By coupling the reduction of Fe^{III} to the oxidation of hydrogen or organic matter they gain energy for growth and the resulting Fe^{II} mainly precipitates in several mineral phases such as magnetite (Fe_3O_4), siderite ($FeCO_3$), chukanovite ($Fe_2OH_2(CO_3)$), vivianite ($Fe_3(PO_4)_2 \cdot 8H_2O$), the

50   hydroxycarbonate green rust 1 ($Fe^{II}_4Fe^{III}_2(OH)_{12}CO_3 \cdot \sim 3H_2O$) and the hydroxysulfate green rust 2 ($Fe^{II}_4Fe^{III}_2(OH)_{12}SO_4 \cdot \sim 8H_2O$) (Lovley *et al.*, 1987; Jorand *et al.*, 2001; Glasauer *et al.*, 2002; Ona-Nguema *et al.*, 2002; Kukkadapu *et al.*, 2005; Zegeye *et al.*, 2005). The nature of the secondary iron mineral is partly controlled by the

presence of its chemical constituents. For instance, phosphate or sulfate are needed

55 to form vivianite or GR2(SO_4^{2-}), respectively. But lower phosphate, concentration (i.e. undersaturated for vivianite precipitation) plays additional role, as organic polymers, bacterial cells or silicate, which is to promote the formation of GR over the magnetite without being constituent of this mineral. Thus, the supplementation of the incubation medium by microbial or synthetic polymers (polyacrylate) or autoclaved cells (Zegeye

60 et al., 2007a; Jorand et al., 2008; O'Loughlin et al., 2010; Zegeye et al., 2010), phosphate (Kukkadapu et al., 2004), quartz particles (SiO_2), silicic acid (H_4SiO_4) or a panel of oxyanions (O'Loughlin et al., 2010; Sergent et al., 2010) significantly promote the formation of GR1 over magnetite from lepidocrocite or ferrihydrite bioreduction.

65 The mechanisms involved in such secondary iron biomineralization remains under investigation. Recently, the organization of mixed aggregates constituted by iron oxide and bacterial cells was proposed to influence the GR vs magnetite mineralization routes (Zegeye et al., 2010). It was suspected that an aggregate constituted by densely packed particles promotes areas at a micro-scale level. These

70 micro-area would exhibit high concentrations of both bicarbonate and Fe^{II}, resulted from the bacterial metabolism, which would explain the formation of GR. Competitive binding site of oxyanions and Fe^{II} onto ferric oxide surface was also suggested as a factor controlling the nature of the bioreduction product (O'Loughlin et al., 2010) as well as the iron reduction rate (Ona-Nguema et al., 2003). In addition, since the

75 carbonated GR1 is relatively unstable as regards to magnetite (Tronc et al., 1992), it has been suggested that the components cited above (phosphate, polymers or silicate), could also promote the formation of GR by playing a protective role on the

4

GR crystals. The sorption of anionic components onto the crystals, especially on the lateral faces, would impair their dissolution and thus their subsequent transformation

80   into magnetite (Benali *et al.*, 2001; Bocher *et al.*, 2004; Sergent *et al.*, 2010).

In natural environments, bacteria are usually present in association with complex organic matter, heterogenous and diverse minerals and inorganic particles. For instance, biofilms, which are a widespread form of life for bacteria, are mainly constituted by an arrangement of bacteria embedded in exo-cellular polymeric

85   substances (EPS) (De Beer and Stoodley, 2006). Thus, since the presence of EPS and large cell densities were identified to be favorable factors for the (bio)mineralization of GR, as afore mentioned, one could expect that biofilms, especially those rich in iron, display a suitable environment for the GR's formation. However, to our knowledge, the formation of GR in a more complex environmental

90   media or from a biofilm material remains poorly studied. Recently, one study has reported the formation of a GR1 by anaerobic incubation of a ferric material collected from a groundwater seep (Blöthe and Roden, 2009).

The purpose of this study was therefore to evaluate the potentiality of a biofilm material to promote the formation of GR and other Fe^{II} phases. To that end, we used

95   ferruginous biofilms present in the Sinnamary Estuary (Atlantic Ocean, French Guiana), a well-described mercury contaminated area, due to past and present anthropic activity (Dominique *et al.*, 2007; Muresan *et al.*, 2008). We evaluated the capability of the biofilm components to display an iron reducing activity and to promote the formation of GR especially because of its high reactivity towards

100 pollutants such as cationic mercury.

5

2. MATERIALS AND METHODS

105 *2.1. Sites and biofilm sampling*

The biofilm samples were collected in the Sinnamary Estuary in French Guiana

(Figure 1) where a hydroelectric dam was built in 1994. The resulting reservoir has

flooded more than 350 km^2 of tropical rainforest inducing a major disturbances of

110 biogeochemical cycles in both the reservoir and the Sinnamary Estuary downstream

the dam (Richard *et al.*, 1997; De Mérona *et al.*, 2005). For example the

biodegradation of the huge immersed biomass has led to a significant decrease of

the E_h in the water column, decreasing the O_2 level from 7.2 mg l^{-1} in 1992 to 0.4 mg l^{-1}

just after the dam from 1995 to present (Richard *et al.*, 1997; Dominique, 2006). As

115 a result, the dam effluent water is significantly concentrated in reduced species such

as soluble Fe^{II} species (up to 15 - 20 μmol l^{-1}) (Muresan *et al.*, 2008) and increased

by a factor 10 (from 2 μmol l^{-1} to 23 μmol l^{-1}) after the dam construction (Dominique,

2006). These Fe^{II} species are probably the precursor of the red flocs transported by

the estuary river and of the thick red-brown slimes recovering any surface in contact

120 with the water up to $\sim$ 30 km after the dam (Figure 2a, b). In addition, the anaerobic

conditions occurring in the reservoir contribute to the formation of the methyl mercury

in the Sinnamary Estuary (Dominique *et al.*, 2007; Muresan *et al.*, 2008).

The samples were collected between March 2005 and March 2008 at three sampling

stations: i) the *Passerelle* station (N5°03'54", W53°03'08"); ii) the *Vénus* station

125 (N5°11'04", 52°58'42") and, iii) the *Estuary* station (N5°26'58", W53°0'21") localized $\sim$

0.8 km, $\sim$ 20 km and $\sim$ 65 km after the Petit-Saut dam respectively (Figure 1).

The biofilms were collected at the *Passerelle* and *Vénus* stations and the surface sediments at the *Estuary* station. They were collected by scrapping the surfaces (immersed rope, branches, rock) with a sterile spoon and poured into sterile boxes in polypropylene filled with the river water. At the *Estuary*, the surface sediments were mainly sand-like deposit (~ 50 cm depth) in the hollow of a rock. The samples were transported to the laboratory station in an isotherm container (Chest 36QT, Coleman[®], Wichita, KS) under one to five hours. Aliquot of these samples were stored in refrigerated conditions (isotherm container with ice-pack, around 4°C) during aircraft transportation to the metropolitan laboratory two weeks after the sampling, or were used on site immediately ("freshly used"). When the samples served both as Fe^{III} source and inocula they were used directly after their collection; when they served as Fe^{III} source only, they were lyophilized after transportation.

2.2. Biomineralization assays

The biomineralization assays were conducted in three ways (Table 1):

- Biofilms as Fe^{III} source: consisted of anaerobic incubations of lyophilized biofilms supplemented with an electron donor and a cell suspension of an iron reducing bacteria.

- Biofilms (or surface sediments) as inocula : consisted of incubations of synthetic lepidocrocite (γ-FeOOH, as Fe^{III} source) with autochtonous bacteria as inoculum and supplemented with an electron donor.

- Biofilms as inocula and Fe^{III} source : consisted of incubations of the fresh biofilm components just supplemented with electron donors.

7

2.3. Biofilms as Fe^{III} source

Dense resting cell suspensions of *Shewanella putrefaciens* CIP80.40 (Collection of Institut Pasteur, Paris, France) were obtained after a 24 h aerobic culture in tryptcase soy broth (30 g l^{-1}, 51019, BioMérieux, Marcy l'Étoile, France) and washed twice (centrifugation 10,000 × *g*; 10 min; 20°C) with 0.7% NaCl solution. A series of duplicates of 100 ml serum bottles (sealed with thick butyl rubber stoppers, Bellco Glass Inc., Vineland, NJ) were prepared and contained 8.4 10^8 and 3.2 10^9 cells ml^{-1} (final concentration) with sodium-formate (NaHCOO) 70 mmol l^{-1} as the sole electron donor in a sterile mineral medium in pure water (MilliRO/MilliQ+, Millipore, Billerica) as previously described (Zegeye *et al.*, 2007a): 22 mmol l^{-1} NH_4Cl, 1.5 mmol l^{-1} NaCl, 1.2 mmol l^{-1} KCl, 1.1 mmol l^{-1} $MgSO_4 \cdot 7H_2O$, 0.71 mmol l^{-1} nitrilotriacetic acid, 0.67 mmol l^{-1} $CaCl_2$, 0.27 mmol l^{-1} $MnSO_4 \cdot H_2O$, 133 μmol l^{-1} anthraquinone disulfonate (ADQS), 86 μmol l^{-1} $ZnCl_2$, 38 μmol l^{-1} $CoSO_4 \cdot 7H_2O$, 32 μmol l^{-1} $FeSO_4 \cdot 7H_2O$, 9.3 μmol l^{-1} $Na_2MoO_4 \cdot 2H_2O$, 9.1 μmol l^{-1} $NiCl_2 \cdot 6H_2O$, 6.8 μmol l^{-1} $Na_2WO_4 \cdot 2H_2O$, 3.6 μmol l^{-1} $CuSO_4 \cdot 5H_2O$, 1.9 μmol l^{-1} $AlK(SO_4)_2 \cdot 12H_2O$, 1.5 μmol l^{-1} H_3BO_3. Finally, 25 g l^{-1} of the lyophilized biofilm were added. The Fe^{III} present in this biofilm (170 mmol l^{-1} Fe^{III} equivalent) was assumed to be the sole electron acceptor. This lyophilized biofilm extract was not heat sterilized in order to avoid any modifications of the iron oxide minerals. All other constituents than lyophilized biofilm and *Shewanella* cells have been heat sterilized, except formate and AQDS which were sterilized by filtration. A control was done in the same conditions except that no resting cells of *S. putrefaciens* was added.

2.4. Biofilms as inocula

One ml of a biofilm suspension collected at *Passerelle* and *Vénus* stations, or from surface sediment (*Estuary* station), served as inoculum for 9 ml of the following anaerobic culture medium (final concentration in purified water): suspension of 5.3 g l^{-1} γ-FeOOH (i.e. : 60 mmol l^{-1} equiv. Fe^{III}) as electron acceptor; 5 mmol l^{-1} sodium formate, 5 mmol l^{-1} sodium acetate, 2.5 mmol l^{-1} sodium lactate as electron donor mix. The basal and mineral medium contained (final concentration in pure water): 30 mmol l^{-1} $NaHCO_3$, 4.5 mmol l^{-1} NH_4Cl, 4 mmol l^{-1} NaH_2PO_4 H_2O, 1.3 mmol l^{-1} KCl, 0.1 mmol l^{-1} $MgSO_4$, 30 μmol l^{-1} $MnSO_4$, 8 μmol l^{-1} $CoSO_4$, 7 μmol l^{-1} $CaCl_2$, 7 μmol l^{-1} $ZnSO_4$, 1.5 μmol l^{-1} H_3BO_3, 1 μmol l^{-1} Na_2SeO_4, 1 μmol l^{-1} $NiCl_2 \cdot 6H_2O$, 0.7 μmol l^{-1} $Na_2WO_4 \cdot 2 H_2O$, 0.5 μmol l^{-1} $Na_2MoO_4 \cdot 2 H_2O$, 0.4 μmol l^{-1} $CuSO_4$, 0.3 μmol l^{-1} $AlK(SO_4)_2 \cdot 12 H_2O$. AQDS (100 μmol l^{-1}) were added with the mix of electron donors, previously sterilized by filtration into the autoclaved medium. Vitamins were added from filtered sterilized stock solutions containing (in final concentration) 20 μg l^{-1} biotin, 20 μg l^{-1} folic acid, 100 μg l^{-1} pyridoxine HCl, 50 μg l^{-1} riboflavin, 50 μg l^{-1} thiamine, 50 μg l^{-1} nicotinic acid, 50 μg l^{-1} pantothenic acid, 1 μg l^{-1} B-12, 50 μg l^{-1} para-aminobenzoic acid, and 50 μg l^{-1} thiotic acid. The lepidocrocite was chemically synthesized according to the method described by Zegeye *et al.* (2007a). Lepidocrocite wad preferentially chosen due to its stability during the heat sterilization of the medium but also because this mineral was suitable for GR biomineralization (Ona-Nguema et al., 2002) and finally because it was identified, as it will be indicated below in the manuscript, to be the main mineral constituting the present ferruginous biofilm.

2.5. Biofilms as inocula and Fe^{III} source

Freshly harvested biofilms from *Passerelle* station were poured into 100 ml serum
bottles filled with the Sinnamary Estuary water (composition described in Table 2).
The suspension obtained was supplemented with 10 – 30 ml of a mix of electron
donors in different proportions (Table 1). It was assumed that the biofilm components
provided the Fe^{III} as the main electron acceptor. At the start of the experiments, the
Fe^{III} amount in the biofilm was not measured yet, therefore three ratio of electron
donor mix / biofilm suspension were tested. The determination of Fe later on
indicated that on the one hand two assays contained 22 and 31 mmol l^{-1} of Fe^{III} with
an electron donor concentration of 4, 4, and 2 mmol l^{-1} for acetate, formate and
lactate respectively; and on the other hand the third assay contained 57 mmol l^{-1} of
Fe^{III} with an electron donor concentration of 15, 15, and 7.5 mmol l^{-1} for acetate,
formate and lactate respectively (Table 1).

All incubation media were purged with O_2-free N_2(99.99%) gas for 30 min in aseptic
condition. All the assays displayed a pH of 6.5±0.2 and were incubated at 30°C in the
dark.

2.6. Analytical techniques

The dry weight (DW) of the biofilm samples were measured in the Hydreco
Laboratory facilities (Kourou, French Guyana) few hours after sampling. The weight
of a desiccated pellets was measured from a 10 ml biofilm suspension centrifuged for
5 min at 10,000 × *g* and dried at 105°C over night. The ash content was measured

after 3 h of calcination (550°C) and the ash free dry weight was then calculated by difference. The total iron content (mg g^{-1} DW) has been performed by ICP-AES after acidic digestion in HCl 6 N.

The Fe^{III} reduction was monitored by measuring the Fe^{II} accumulation over time. The amount of total Fe^{II} (*i.e.* in the solid and soluble phases) extracted by HCl 5 mol l^{-1} was determined with ortho-phenanthroline (Fadrus and Maly, 1975). The soluble Fe^{II} was assessed after filtration through 0.2 μm membrane filter (Millex-GP SLGP, Millipore, Billerica, MA) in an anaerobic chamber (N$_2$/H$_2$, 97/3, Coy Laboratory Product Inc., Grass Lake, MI, USA).

The cell numbers were determined by the epifluorescence microscopy technique using the SYBR green I fluorochrome as a dye (InVitrogen) on the biofilm suspension, previously dispersed by ultrasonic bath treatment (15 min, 120 W, RK31, 35KHz, Sonoclean, Paris, France).

2.7. Solid analysis

Surface elemental composition of the lyophilized biofilm has been determined by X-ray photoelectron spectroscopy (XPS). XPS spectra were recorded using a KRATOS Axis Ultra spectrometer instrument with a monochromatic Al Kα Xray (hν = 1486.6 eV) with the same procedure and apparatus than Zegeye *et al.* (2007b).

The solids were also characterized by X-ray diffraction (XRD), transmission electron microscopy (TEM), scanning electron microscopy (SEM), Raman spectroscopy (RS), and Mössbauer spectroscopy (MS). The XRD data were collected with a D8 Bruker diffractometer, equipped with a scintillator detector. The X-ray source was a Co

250   anode (λ = 0.17902 nm). The diffractograms were recorded in the $3 - 64°$ 2θ range,

with a 0.035° step size and a collecting time of 3 seconds per point.

The suspension was filtered under N_2 atmosphere, mixed with glycerol to avoid

oxidation and placed on a sample carrier to be analyzed by XRD.

For TEM observation, one drop of the suspension was laid on an amorphous carbon-

255   coated grid and the sample was loaded into the microscope (Philips CM20/STEM).

The relative element composition of the analyzed solids was obtained by energy

dispersive X-ray analysis (EDX). For the scanning electronic microscopy (SEM)

examination, one drop of the sample was sprinkled onto 2 cm^2 plates and examined

under vacuum (Hitachi 54800 Scanning Electron Microscopy).

260   A Raman characterization was performed with a special cell used for Raman

experiments. The sample was set under an N_2-O_2 free atmosphere in an anaerobic

chamber and the cell was tightly closed by a glass window through which a laser

beam was focused and the Raman backscattering collected. The cell is mounted in

the focal plane of an Olympus B.H. microscope in a Jobin-Yvon/Instrument S.A. T

265   64000 Raman microprobe equipped with charged coupled device detector and a

motorized X-Y stage. A large working distance objective length of 50 x magnification

was used. A 514.53 nm exciting radiation was used with a power ~0.2 mW to prevent

sample degradation. The spectra resolution was about of 6 cm^{-1} and the precision on

the wavenumber was 1 cm^{-1}. Two successive scan of 90 s were performed.

270   The Mössbauer spectroscopy (MS) was performed from 12 to 295 K with a closed

helium cycle variable temperature Mössbauer cryostat equipped with vibration

isolation stand manufactured by Advanced Research Systems (ARS), utilizing a

constant acceleration Mössbauer spectrometer with a 50 mCi source of ^{57}Co in Rh

12

and calibrated with a 25 μm thick a-Fe foil at ambient temperature. Spectra were

275　fitted using Lorentzian-shape lines and parameters were mathematically

(minimization of χ^2) and physically significant.

2.8. Microscopy for cells and biofilm matrix observations

280　The embedding technique previously described by Droppo *et al.* (1996) has been

modified and adapted to the ferruginous biofilms. Briefly, freshly handled fragments

of biofilms with their substrata (nylon rope) were poured into 10 ml of estuarine water

containing 4 % of glutaraldehyde. After the settlement of the fragments (~ 2 h), the

supernatant was gently removed and replaced by a solution of low-melting-point

285　electrophoresis grade and sterile agarose (0.75 %). After solidification (and

transportation until the metropolitan laboratory in isotherm boxes) the samples were

dewatered in ethanol and in propylene oxide, and embedded in epoxy resin. Finally,

thin and ultra-thin sections were stained with Azur blue II or lead nitrate respectively

prior to examination with the optical microscopy or TEM respectively.

290

3. Results

3.1. Characterization of the ferruginous biofilms

295

The biofilm recovering all surfaces in contact with the water of the Sinnamary Estuary

appeared as a brown-orange color gluying slime (Figure 2a, b) being in some areas

up to ~1 cm thick. As expected, iron was the major inorganic part of the biofilms from

Passerelle and *Vénus* stations and accounted for 0.37 and 0.20 g g^{-1} of the dry

13

300   weight according to ICP-AES analysis, respectively (Table 2). The XPS analysis

confirmed the presence of an important amount of iron into the biofilm. The oxide

component located at 530.9 eV in the O_1s spectrum (Table SI-1) indicated that the

iron was involved in a ferric oxide phase. The organic matter represented approx. 35

% of the DW part of the ash free dry weight measure (Table 2). In addition to oxygen,

305   the significant amount of N, C and S was in agreement with the presence of organic

matter. Optical microscopic observation indicated the presence of copious amount of

various microorganisms like diatoms (not shown) and bacterial colonies embedded in

an organic or Fe-bearing gel like matrix (Figure 2c). Iron oxides were present in close

vicinity to bacterial cells (Figure 2d).

310   The Table 2 indicates that microbial cells accounted for a significant part of the

biofilm constituents with $1.3 - 6 \times 10^{11}$ cells g^{-1} DW. According to their composition

these biofilms can be well qualified as a ferruginous one.

TEM and XRD analyses of the inorganic phases indicated amorphous or slightly

diffracting materials. Two Fe-phases were discerned. The first one showed a

315   "crumpled paper" like structure, and gave an electron diffraction pattern consistent

with the lepidocrocite (γ-FeOOH) (Fig. 2e and Table SI-2). The X-ray diffraction

pattern exhibited the major band specific to SiO_2 but also very broad bands localized

in the same area of those of lepidocrocite and in a lower trend of ferrihydrite (Fig. 3a).

The second Fe-phase did not display a diffraction spectrum with the electron beam

320   and exhibited a granular trend (Fig. 2f). Fe and O were the major elements of those

two phases, along with Si, Al, Na, and Cl in a lower amount according to EDX

analysis (not shown). The presence of both γ-FeOOH and ferrihydrite was in

agreement with Raman spectroscopy analyses. The spectrum of the lyophilized

14

biofilm (spectra *a* in Fig. 3b) shows band at 250 cm^{-1}, a broad band in the area of 375

325   cm^{-1} and a very broad band in the area of 700 cm^{-1} matching well with the spectra of

synthetic lepidocrocite and ferrihydrite (spectra *c* and *b*, respectively) (Fig. 3b).

The room temperature Mössbauer spectrum of the ferruginous biofilms exhibited a

broadened doublet, which can be fitted reasonably with two paramagnetic

quadrupole components D_L and D_F (Fig. SI-3). The two doublets were distinct in their

330   quadrupole splittings (0.55 and 0.91) whereas their isomer shifts were identical.

According to the literature, the component D_L (Table SI-3) characterized by the

isomer shift of 0.33 and the quadrupole splitting of 0.55 mm/s corresponds to

lepidocrocite (Murad and Schwertmann, 1984). The other component D_F, with the

same isomer shift (0.35 mm/s), and a larger quadrupole splitting of 0.91 mm/s

335   characterizes ferryhydrite. The Mössbauer spectroscopy confirmed therefore that

lepidocrocite and ferrihydrite were the main Fe^{III} oxides of the biofilm. In addition, it

enlighten that lepidocrocite and ferrihydrite contributed to 3/4 (74 %) and 1/4 (26 %)

of the whole solid Fe phase, respectively (Table SI-3).

340   *3.2. Bioreduction of Fe^{III} material*

Up to 63 % of the lyophilized ferruginous biofilm's Fe^{III} were reduced by *S.*

putrefaciens after 70 days of incubation (Table 1 and Fig. 4). After 800 days, the

amount of Fe^{II} formed did not change indicating that the equilibrium in term of Fe^{II}

345   level was attained after 70 days. A slight Fe^{III} reduction was noted in the control

(without *Shewanella* cells) (Fig. 4) probably due to a residual activity of iron reducing

bacteria in the lyophilized sample. This was supported by the growth of some

colonies in anaerobic as well as in aerobic incubation on solid medium (TS agar) (not

15

shown). Thus, it indicates that at least 2/3 of the total Fe was available for

350 bioreduction. In addition, no significant difference, in terms of iron reduction extent

and initial iron reduction rate (16 ± 4 mmol l^{-1} day^{-1}, from data of Fig. 4 fitted as a first

order kinetic) was clearly evidenced between the assays containing 8.4×10^8 cells ml^{-1}

(named LC for "low" cell density) and those with 3.2×10^9 cells ml^{-1} (named HC for

"high" cell density) (Fig. 4).

355 The "aqueous Fe^{II}" (< 0.2 μm) was very low in all samples (< 20 μmol l^{-1}) (at 70 days)

clearly indicating that Fe^{II} was mainly under a solid state.

3.3. Ability of autochtonous cells to reduce iron oxide

360 After six months of incubation time, up to 39% of γ-FeOOH were reduced by the

biofilm (*Passerelle* and *Vénus*) and the surface sediment (*Estuary*) aliquots indicating

the presence of iron reducing bacteria in those samples (Table 1). The anaerobic

incubation of the freshly sampled biofilm supplemented with electron donor mix (that

is to say the fresh biofilm served both as iron oxide and iron reducing bacteria

365 sources), revealed the reduction of $59 \pm 6\%$ of the ferric oxides after 180 days (Table

1). An increase of nearly two units of pH was noted (6.5 to 8.5, Table 1) as it is

usually observed during the Fe^{III} reduction in weakly buffered medium (Ona-Nguema

et al., 2002; Zegeye *et al.*, 2007a).

Therefore, the biofilms and surface sediment samples exhibited an efficient iron

370 reducing activity to reduce up to 2/3 of the endogenous Fe^{III} or exogenic iron oxide

(synthetic lepidocrocite).

16

3.4. Characterization of the secondary iron minerals

375   The analysis by XRD and TEM of the solid phase clearly indicated the presence of

GR1 in both the incubation assays when the biofilm served as Fe^{III} source

(lyophilized biofilm inoculated with *S. putrefaciens*) and as inocula (synthetic

lepidocrocite inoculated with 10% v/v fresh sample extract) (Table 1).

In the first case the GR1 was identified by XRD, TEM and MS after 70 and 800 days

380   of incubation as the major solid Fe phase for the two cell concentrations tested. XRD

displayed no other characteristic and significant peaks, except a weak one for

magnetite, than those of the GR1 after 70 days (Fig. 5) indicating that the GR1 was

the major ferrous crystalline phase. However, in the LC (low cell density) assays, the

GR1 signal intensity appeared lower suggesting a poor crystallinity of the solids in

385   those samples. After 800 days of incubation, the GR1 still remained the major

crystalline phase (at a level discernable by XRD) despite of a stronger signal

intensities for the magnetite and the apparition of a calcium magnesium iron

carbonate. In the control, no significant peak was detected (Fig. 5). The TEM

examination showed crystals with a rounded shape (Fig. 6a), and by SEM they

390   looked-like amorphized GR platelet (Fig. 6b). Those crystals exhibited a diffraction

pattern characteristic of the GR1 (Fig. 6a and Table SI-4). The Mössbauer spectrum

at room temperature (Fig. SI-3) displayed a mixture of a component (four doublets in

the center of the spectrum) in a paramagnetic state and at higher energy, two sextets

S_1 and S_2 in magnetically ordered states. Theses sextets were attributed respectively

395   to iron in tetrahedral (Fe^{3+}) and octahedral ($Fe^{2.5+}$) sites in the magnetite crystal. The

intensity ratio between S_1 and S_2 of about 2 concurred likely with a stoichiometric

magnetite. The four doublets obtained in the center of the spectrum correspond to

17

two Fe^{2+} doublets (large values of quadrupole splitting and isomer shift) and to two Fe^{3+} doublets (small value of quadrupole splitting an isomer shift). The hyperfine

400   parameters (Table SI-5) confirmed the presence of the GR in this sample (Refait *et al.*, 2006), thus supporting the diffraction results (XRD and TEM). The Mössbauer spectroscopy confirmed also the presence of another Fe^{II} bearing mineral (probably the calcium magnesium iron carbonate) and indicated a remaining of Fe^{III} source. The three phases, GR, magnetite and calcium magnesium iron carbonate counted for

405   60%, 20% and 13% of the total iron respectively. The fourth phase, the residual lepidocrocite, accounted for 7% (Table SI-5).

In the second case (assays with biofilms as inocula for synthetic lepidocrocite reduction), some GR crystals were observed by optical microscopy or by TEM examination (Fig. 6c&d) and XRD analysis confirms the presence of GR phase with

410   vivianite ($Fe_3(PO_4)_2 \cdot 8H_2O$) (Fig. SI-4) due likely to the presence of phosphate in the culture medium.

The observation by optical microscopy of the solids from the incubation with biofilm serving both as electron acceptor and inoculum, showed several green rust-like colored particles (Fig. 6f). In order to discriminate those particles with cell-bearing

415   chlrorophyll, the suspension was examined under UV light. Some green particles were red fluorescent corresponding to photosynthetic cells, but other green particles were non-fluorescent under UV light excluding the fact that they correspond to cell-containing chlorophyll. Particles exhibiting the same size ($\sim 1 \mu m$) were observed under TEM. They gave an electronic diffraction pattern corresponding to an

420   hexagonal symmetry (Fig. 6e) and the other 1.6 time higher than the d_{hkl} {101} exhibiting (0.441 nm against 0.272). TEM-EDX indicated that these particles were

constituted by 34±2 % and 66±2% of Fe and O, respectively. However, the other

solid analysis methods, like XRD, Raman spectroscopy or MS, did not provide any

exploitable results due probably to the low amount of samples in the assays.

425

4. Discussion

4.1. Ferric iron oxides and bacteria in the biofilm

430 A growing body of literature indicates that biofilm materials, cell surface appendages

or exo-polymeric substances contribute significantly to the secondary iron

biomineralization (Ferris et al., 1986; Brown et al., 1994; Brown et al., 1998; Salas *et

al.*, 2010). The most accepted mechanism is that cell surface could play the role of

nucleation center to initiate the crystal formation. In addition, specific cellular

435 metabolism could also be involved acting as iron oxidizer or reducer. The biofilms

developing in the Sinnamary Estuary, would then present a suitable environment for

such mineralization processes. They are indeed mainly constituted of iron (30-40% of

the DW) and microbial cells. The two iron oxides identified in these biofilms,

lepidocrocite and ferrihydrite, could result from physico-chemical reactions or be

440 induced by bacterial activity. The ferrihydrite is a widespread iron oxide and also

precipitates in the vicinity of iron oxidizing bacteria (Fortin and Langley, 2005).

Lepidocrocite one the other hand, is a relatively scarce iron oxide, it has however a

widespread occurrence in suboxic environment such as reductomorphic soils and it is

a typical oxidation product of GR (Schwertmann and Taylor, 1989). It was also shown

445 to be the main product of Fe^{II}-oxidizing nitrate reducing bacteria (Larese-Casanova *et

al.*, 2010).

In the biofilms used in the present work, the lepidocrocite exhibited low sized crystals and a weak cristallinity (according to the broad XRD peaks) and the ferrihydrite was not detected by XRD. Such characteristics are typical of natural iron oxides

450 associated with high organic matter, especially for the bacteriogenic ferric iron oxides resulting from a rapid Fe^{II} oxidation (Schwertmann and Taylor, 1989 ; Fortin and Langlet, 2005). Moreover, twisted like structures (Fig. SI-5) suggest the presence of *Gallionella* sp., a ferrous oxidizing bacteria genous (Ghiorse and Ehrlich, 1992). The low acidic pH ($\sim$ 6.5) and the significant level of Fe^{2+} occurring in the Sinnamary

455 estuarine water are also favorable conditions for near-neutral iron oxidizing bacteria (Søgaard *et al.*, 2000 ; Blöthe an Roden, 2009). The bacteria are embedded into an EPS matrix and are in close contact with iron solids supporting the hypothesis of a direct interaction between bacteria and iron oxides. These iron oxides could be the by-product of iron oxidizing bacteria, and could also serve as final electron acceptor

460 for DIRB (Straub *et al.*, 1998). Indeed, the iron reducing bacteria were estimated to represent up to 10^8 cells g^{-1} in those biofilms (Huguet *et al.*, 2010). As it is usually observed for mature biofilms or bacterial aggregates, the aerobic metabolism of bacteria could significantly affect the redox potential and create strong anaerobic conditions few dozen or hundred μm within a biofilm (Stewart and Franklin, 2008)

465 which would allow the anaerobic respiration of Fe^{III} and subsequently the formation and the stability of secondary Fe^{II}-bearing minerals. The possibility that bacterial Fe^{II} oxidation and Fe^{III} reduction could be tightly coupled in such environments have been suggested and documented (Emerson and Mayer, 1997; Sobolev and Roden, 2002; Blöthe and Roden, 2009).

470

4.2. Iron reduction and GR biomineralization

In order to evaluate the capability of biofilm's iron oxides to be transformed into

secondary iron minerals, lyophilized biofilm were used as electron acceptor for *S.*

475 *putrefaciens*, a bacteria well-known to precipitate GR from lepidocrocite or ferrihydrite

bioreduction. The iron reduction rates (0.7 ± 0.1 mmol l^{-1} h^{-1} from data of Fig. 4) of the

ferric material present in the Sinnamary biofilm were in the same order of magnitude

comparatively to other studies performed in similar conditions in terms of cells/Fe^{III}_s

ratio and formate concentration (iron reduction rate varied from ~ 0.1 to 15 mmol L^{-1}

480 h^{-1}, Ona-Nguema *et al.*, 2002 ; Zegeye *et al.*, 2007a; O'Loughlin *et al.*, 2007;

O'Loughlin *et al.*, 2010; Zegeye *et al.*, 2010). This indicates that the ferric oxides of

the biofilms from the Sinnamary River were readily available for bacterial reduction.

Indeed, as regards to the proportion of Fe^{III} reduced, the ferric biofilm material

appeared to be more reducible than the synthetic iron oxide (Table 1). This was also

485 noted from previous studies with natural ferric material from another origin (Straub *et*

al., 1998; Blöthe and Roden, 2009). The GR1 (assumed to be the $GR(CO_3^{2-})$) was the

main secondary mineral produced by the bacterial reduction of the biofilm's iron oxide

by *S. putrefaciens*. It has been previously shown that *S. putrefaciens* CIP 80.40

promotes the GR biomineralization under a high ratio cell density/iron oxide (above

490 10^{10} mmol^{-1}) (Zegeye *et al.*, 2007a; Zegeye *et al.*, 2010). At a lower ratio cells/Fe^{III}

and in absence of significant amount of phosphate or silica, magnetite (Fe_3O_4) was

the main secondary mineral expected as regards to literature data (Fredrickson *et al.*,

1998; Ona-Nguema *et al.*, 2002; Kukkadapu *et al.*, 2004; Zegeye *et al.*, 2007a;

Zegeye *et al.*, 2010; Sergent *et al.*, 2010). In the present work, whatever the ratio

495 used, below (0.5×10^{10} mmol^{-1}) or above (2×10^{10} mmol^{-1}), the GR was the dominant

21

secondary iron mineral with minor magnetite formation as indicated by Mössbauer

analysis. This indicates that the lyophilized biofilm promotes the GR1 instead of

magnetite. The lyophilized biofilm contains a large proportion of organic matter like

cellular wastes and probably exo-cellular polymers. Thus, in previous works, it was

500 shown that autoclaved cells, EPS or organic polymers promote the GR precipitation

(Zegeye *et al.*, 2007a; Jorand *et al.*, 2008; O'Loughlin *et al.*, 2010). Flocculation and

bacterial strains have been also suggested to influence the GR precipitation (Salas *et*

al., 2010; Zegeye *et al.*, 2010). Similar results concerning the secondary mineral

were obtained from ferruginous biofilm ("layered natural ferric precipitates") collected

505 from a groundwater seep (Blöthe and Roden, 2009). Therefore, ferruginous biofilms

like those found into the Sinnamary Estuary are expected to be favorable for the

precipitation of GR since they exhibit EPS and large cell density in a close volume.

4.3. Green rust ageing and stabilization

510

The stability of carbonated GR1 is known to be very weak in the absence of

stabilizing agents like phosphate, microbial cell suspension, or silicate and is readily

transformed, within few hours, into magnetite (Benali *et al.*, 2001; Bocher, *et al.*,

2004; Kukkadapu *et al.*, 2005). The XRD analysis of aged incubation samples at

515 30°C in darkness during 800 d (~ 2 years) showed that the GR1 is still present after a

long period of time in the medium, indicating the relative stability of the mineral in

those conditions. Only a minor fraction of GR was partially transformed into

magnetite and/or calcium magnesium ferrous carbonate. This suggest that the

biofilms or the medium (e.g. : phosphate in that case) have provided some materials

520 inducing the stabilization of the GR1.

22

It is wellknown that the GR is readily produced from γ-FeOOH bioreduction in batch experiment with a large cell density of pure strain *Shewanella* sp. (resting cells). This has been also shown by this work with environmental iron oxides. But when the cell density was lower, i.e. in order to initiate a cell growth or to start with a cell density closer to that found in natural environments (i.e. $< 10^8$ cells mL^{-1}), the extent of the Fe^{III} reduction was generally very low and the number of cultivable cells declined with the time (e.g. : Roden and Urrutia, 2002). For such studies, the final product was mainly the magnetite (e.g. : Lovley *et al.*, 1987; Glasauer *et al.*, 2003). However, it was reported by Blöthe and Roden (2009) and from the present study, that the formation of GR1 occurred from environmental sample where the Fe oxide appears to be associated with organic phases. The key role of the organic phases would proceed by stabilizing the GR1 or by initiating its formation instead of another Fe^{II} bearing mineral.

The organic material associated with the biofilm as well as constituents such as humic-like substances, quartz particles could contribute to GR occurrence as it was suggested by laboratory experiments (O'Loughlin et al., 2010; Sergent et al., 2010). These hypothesis need however to be supported by more data on the nature of the dominate members of the microbial community responsible for the Fe^{III} reduction and for the GR formation.

4.4. GR occurrency in Sinnamary Estuary and biofilms

The formation of Fe^{II}-bearing minerals, especially the GR mineral can be expected in the biofilm of the Sinnamary river since several conditions are gathered to allow its synthesis: presence of DIRB activity into the biofilm, a readily reducible ferric oxides.

23

Moreover, the pH interval of the Estuary water is close to the pH (H_2O) of the hydromorphic soils where the GR mineral (fougerite) has been identified (Bourrié *et al.*, 1999). However, the mineral has not been yet detected directly in the raw biofilm. One can hypothesize that the GR could be present at very low concentration, below the detection level, or it was oxidized during sampling and/or transportation. The causes could be a lack of electron donor or/and a too high O_2 level. Nevertheless, the ferric materials and bacteria constituting these biofilms can potentially support the biomineralization of such interesting mineral serving as electron donor for oxidized chemicals. By extension, one can assume that biofilm could represent an efficient substrate for GR formation. One could speculate that in mercury contaminated area such as the Sinnamary Estuary, the GR has to be taken into account as a potential abiotic mercury attenuation mean of the water phase.

5. Conclusions

The anaerobic incubation of ferruginous biofilm components with a pool of electron donor can lead to the formation of the Fe^{II}-Fe^{III} hydroxysalt green rust from the activity of iron reducing bacteria. In addition, this green rust exhibited a great stability (over than three years in the batch incubation) in the aqueous suspension probably due to the polymeric materials which contribute likely to its stability. The biofilms, such those found in the anthropised Sinnamary Estuary in French Guyana, should therefore be considered as a favorable location for GR biomineralization when redox conditions and electron donors availability are gathered. The presence of this mineral is expected to be in anaerobic pockets within the biofilms, and dedicated analysis on fresh biofilms, preserved from air oxidation, could be conducted to support this

570   hypothesis. Moreover, this ferrous mineral could also serve as Fe^{II} source for iron

oxidizing bacteria and thus be involved in a cycling of iron at a microscopic scale.

Finally, if the presence of green rust in such biofilm is confirmed, it would contribute

to the mercury attenuation, which is a pollutant of a major concern in the Sinnamary

Estuary, by reducing the Hg^{II} into the volatile $Hg°$.

575

575

References

590   Ahmed IMAM, Benning LG, Kakonyi G, Sumoondur AD, Terrill NJ, Shaw S.
Formation of green rust sulfate: a combined in situ time-resolved X-ray scattering
and electrochemical study. Langmuir 2010; 26:6593-603.

Benali O, Abdelmoula M, Refait P, Génin JM. Effect of orthophosphate on the
oxidation products of Fe(II)-Fe(III) hydroxycarbonate : the transformation of green
595   rust to ferrihydrite. Geochim Cosmochim Acta 2001; 65:1715-26.

Blöthe M, Roden EE. Microbial iron redox cycling in a circumneutral-pH groundwater
seep. Appl Environ Microbiol 2009; 75:468-73.

Bocher F, Gehin A, Ruby C, Ghanbaja J, Abdelmoula M, Génin JM. Coprecipitation
of Fe(II-III) hydroxycarbonate green rust stabilised by phosphate adsorption. Solid
600   State Sci 2004; 6:117-24.

Bourrié G, Trolard F, Génin JMR, Jaffrezic A, Maître V, Abdelmoula M. Iron control
by equilibria between hydroxygreen rusts and solutions in hydromorphic soils.
Geochim Cosmochim Acta 1999; 63:3417-27.

Brown DA, Kamineni DC, Sawicki JA, Beveridge TJ. Minerals associated with
605   biofilms occurring on exposed rock in a granitic underground research laboratory.
Appl Environ Microbiol 1994; 60:3182-91.

Brown DA, Beveridge TJ, Keevil CW, Sherriff BL. Evaluation of microscopic
techniques to observe iron precipitation in a natural microbial biofilm. FEMS
Microbiol Ecol 1998; 26:297-310.

610   Christiansen BC, Balic-Zunic T, Dideriksen K, Stipp SLS. Identification of green rust
in groundwater. Environ Sci Technol 2009; 43:3436-41.

De Beer D, Stoodley P. Microbial biofilms. Prokaryotes 2006; 1:904-37.

De Mérona B, Vigouroux R, Tejerina-Garro FL. Alteration of fish diversity
downstream from Petit-Saut Dam in French Guiana. Implication of ecological
615   strategies of fish species. Hydrobiologia 2005; 551:33-47.

Dominique Y. Contamination par les différentes formes chimiques du mercure de la
composante biologique du barrage hydroélectrique de Petit-Saut et des zones
amont/aval du fleuve Sinnamary, en Guyane francaise (études <u>in situ</u> et approches

expérimentales). 2006. PhD Thesis, University Bordeaux 1, Bordeaux, France, 366
620   pages.

Dominique Y, Maury-Brachet R, Muresan B, Vigouroux R, Richard S, Cossa D et al.
Biofilm and mercury availability as key factors for mercury accumulation in fish
(*Curimata cyprinoides*) from a disturbed Amazonian freshwater system. Environ
Toxicol Chem 2007; 26:45-52.

625   Droppo IG, Flannigan DT, Leppard GG, Jaskot C, Liss SN. Floc stabilization for
multiple microscopic techniques. Appl Environ Microbiol 1996; 62:3508-15.

Emerson D, Moyer C. Isolation and characterization of novel lithotrophic iron-
oxidizing bacteria that grow at circumneutral pH. Appl Environ Microbiol 1997;
63:4784-92.

630   Erbs M, Hansen HCB, Olsen CE. Reductive dechlorination of carbon tetrachloride
using iron(II) iron(III) hydroxide sulfate (green rust). Environ Sci Technol 1999;
33:307-11.

Fadrus H, Maly J. Suppression of iron(III) interference in the determination of iron(II)
in water by the 1,10-phenanthroline method. Analyst 1975; 100:549-54.

635   Ferris FG, Beveridge TJ, Fyfe WS. Iron-silica crystallite nucleation by bacteria in a
geothermal sediments. Nature 1986; 320:609-11.

Fortin D, Langley S. Formation and occurrence of biogenic iron-rich minerals. Earth-
Sci Rev 2005; 72:1-19.

Fredrickson JK, Zachara JM, Kennedy DW, Dong H, Onstott TC, Hinman NW et al.
640   Biogenic iron mineralization accompanying the dissimilatory reduction of hydrous
ferric oxide by a groundwater bacterium. Geochim Cosmochim Acta 1998; 62:19-
20.

Génin JMR, Aissa R, Gehin A, Abdelmoula M, Benali O, Ernsten V et al. Fougerite
and Fe(II-III) hydroxycarbonate green rust: ordering deprotonation and/or cation
645   substitution; structure of hydrotalcite-like compounds and mythic hydroxide Fe(OH)
(2+x). Solid State Sci 2005; 7:545-72.

Ghiorse WC, Ehrlich HL. Microbial biomineralization of iron and manganese. In:
Skinner HCW, Fitzpatrick RW, editors. Biomineralization. Processes of iron and
manganese. Cremlingen, Germany: Catena Verlag; 1992. p. 75-99.

650   Glasauer S, Langley S, Beveridge TJ. Intracellular iron minerals in a dissimilatory iron-reducing bacterium. Science 2002; 295:117-19.

Glasauer S, Weidler PG, Langley S, Beveridge TJ. Controls on Fe reduction and mineral formation by a subsurface bacterium. Geochim Cosmochim Acta 2003; 67:1277-88.

655   Herbillon A. Ferrosic hydroxides, green rusts and fougerite in the biogeochemical cycle of iron. CR Geosci 2006; 33:393-401.

Huguet L, Castelle S, Schäfer J, Blanc G, Maury-Brachet R, Reynouard C et al. Mercury methylation rates of biofilm and plankton microorganisms from a hydroelectric reservoir in French Guiana. Sci Total Environ 2010; 408:1338-48.

660   Jorand F, Appenzeller B, Abdelmoula M, Refait P, Block JC, Génin JMR. Assessment of vivianite formation in *Shewanella putrefaciens* culture. Environ Technol 2000; 21:1001-05.

Jorand F, Landry F, Zegeye A, Lartiges B, Mustin C. Monitoring green rust biomineralization with polymer addition. Geophysical Research Abstracts, Vol. 10,
665   EGU General Assembly; 2008.

Kukkadapu RK, Zachara JM, Fredrickson JK, Kennedy DW. Biotransformation of two-line silica-ferrihydrite by a dissimilatory Fe(III)-reducing bacterium: formation of carbonate green rust in the presence of phosphate. Geochim Cosmochim Acta 2004; 68:2799–814.

670   Kukkadapu RK, Zachara JM, Fredrickson JK, Kennedy DW, Dohnalkova AC, Mccready DE. Ferrous hydroxyl carbonate is a stable transformation product of biogenic magnetite. Am Mineral 2005; 90:510-15.

Larese-Casanova P, Haderlein SB, Kappler A. Biomineralization of lepidocrocite and goethite by nitrate-reducing Fe(II)-oxidizing bacteria: effect of pH, bicarbonate,
675   phosphate and humic acids. Geochim Cosmochim Acta 2010; 74:2799-814.

Lovley DR, Stolz JF, Nord Jr GL, Phillips EJP. Anaerobic production of magnetite by a dissimilatory iron-reducing microorganism. Nature 1987; 330:252-54.

Loyaux-Lawniczak S, Refait P, Ehrhardt JJ, Lecomte P, Génin JMR. Trapping of Cr by formation of ferrihydrite during the reduction of chromate ions by Iron (II)-Iron(III)
680   hydroxysalt green rusts. Environ Sci Technol 2000; 34:438-43.

Murad E, Schwertmann U. The influence of crystallinity on the Mössbauer spectrum of lepidocrocite. Mineral Mag 1984; 48:507-11.

Muresan B, Cossa D, Coquery M, Richard S. Mercury sources and transformations in a man-perturbed tidal estuary; the Sinnamary Estuary, French Guiana. Geochim Cosmochim Acta 2008; 72, 5416-30.

Myneni SCB, Tokunaga TK, Brown Jr GE. Abiotic Se redox chemistry in the presence of Fe(II, III)-oxides. Science 1997; 278:1106-09.

O'Loughlin EJ, Kelly SD, Kemner KM, Csencsits R, Cook RE. Reduction of Ag[I], Au[III], Cu[II], and Hg[II] by Fe[II]/Fe[III] hydroxysulfate green rust. Chemosphere 2003; 53:437-46.

O'Loughlin EJ, Larese-Casanova P, Scherer M. Green rust formation from the bioreduction of γ-FeOOH (lepidocrocite): comparison of several *Shewanella* species. Geomicrobiol J 2007; 24:211-30.

O'Loughlin EJ, Gorski CA, Scherer MM, Boyanov MJ, Kemner KM. Effects of oxyanions, natural organic matter, and bacterial cell numbers on the bioreduction of lepidocrocite (γ-FeOOH) and the formation of secondary mineralization products. Environ Sci Technol 2010; 44:4570-76.

Ona-Nguema G, Abdelmoula M, Jorand F, Benali O, Géhin A, Block JC et al. Iron (II,III) hydroxycarbonate green rust formation and stabilization from lepidocrocite bioreduction. Environ Sci Technol 2002; 36:16-20.

Ona-Nguema G, Benali O, Jorand F, Abdelmoula M, Block JC, Génin JMR. Key role of the kinetics of γ-FeOOH bioreduction on the formation of Fe(II)-Fe(III) minerals. Proc. of the International Conference on the Applications of the Mössbauer Effect. Hyperfine Interact (C) 2003; 5:415-18.

Refait P, Simon L, Génin JMR. Reduction of SeO_4^{2-} anions and anoxic formation of iron(II)-iron(III) hydroxy selenate green rust. Environ Sci Technol 2000; 34:819-25.

Refait P, Abdelmoula M, Génin JMR, Sabot R. Green rusts in electrochemical and microbially influenced corrosion of steel. CR Geosci 2006; 338:476-87.

Richard S, Arnoux A, Cerdan P. Evolution in physico-chemical water quality in the reservoir and downstream following the filling of Petit Saut dam (French Guiana). Hydroécologie Appliquée 1997; 9(1-2):57-83.

Roden EE, Urrutia MM. Influence of biogenic Fe(II) on bacterial crystalline Fe(III) reduction. Geomicrobiol J 2002; 19:209-51.

Salas EC, Berelson WM, Hammond DE, Kampf AR, Nealson KH. The impact of bacterial strain on the products of dissimilatory iron reduction. Geochim Cosmochim Acta 2010; 74:574-83.

Schwertmann U, Taylor RM. Iron oxides. In: Dixon JB, Weed SB, editors. Minerals in soil environments. Madison, WI: Soil Science Society of America; 1989. p. 379-438.

Sergent AS, Jorand F, Hanna K. Biomineralization of Fe^{II}-Fe^{III} species in porous heterogeneous medium of sand/iron oxyhydroxide/bacteria. Proc. of Goldschmidt conference, « Earth, energy and the environment », Knoxville, Tennessee, June 13th – 18th; 2010.

Sobolev D, Roden EE. Characterization of a neutrophilic, chemolithoautotrophic Fe(II)-oxidizing ß-proteobacterium from freshwater wetland sediments. Geomicrobiol J 2004; 21:1-10.

Søgaard EG, Medenwaldt R, Abraham-Peskir JV. Conditions and rates of biotic and abiotic iron precipitation in selected Danish freshwater plants and microscopic analysis of precipitate morphology. Water Res 2000; 34:2675-82.

Stewart PS, Franklin MJ. Physiological heterogeneity in biofilms. Nat Rev Microbiol 2008; 6:199-210.

Straub KL, Hanzlik M, Buchholz-Cleven BEE. The use of biologically produced ferrihydrite for the isolation of novel iron-reducing bacteria. Syst Appl Microbiol 1998; 21:442-49.

Tamaura Y, Ito K, Katsura T. Transformation of γ-FeOOH to Fe$_3$O$_4$ by adsorption of iron(II) ion on γ-FeOOH. J Chem Soc, Dalton T 1983; 1983:189-94.

Trolard F, Génin JMR, Abdelmoula M, Bourrié G, Humbert B, Herbillon AJ. Identification of a green rust mineral in a reductomorphic soil by Mössbauer and Raman spectroscopies. Geochim Cosmochim Acta 1997; 61:1107-111.

Trolard F, Bourrié G, Abdelmoula M, Refait P, Feder F. Fougerite, a new mineral of the pyroaurite-iowaite group: description and crystal structure. Clay Clay Miner 2007; 55:323–34.

Tronc E, Belleville P, Jolivet JP, Livage J. Transformation of ferric hydroxide into spinel by FeII adsorption. Langmuir 1992; 8:313-19.

Zegeye A, Ona-Nguema G, Carteret C, Huguet L, Abdelmoula M, Jorand F. Formation of hydroxysulphate green rust 2 as a single iron(II-III) mineral in microbial culture. Geomicrobiol J 2005; 22:389-99.

Zegeye A, Ruby C, Jorand F. Kinetic and thermodynamic analysis during dissimilatory γ-FeOOH reduction: formation of green rust 1 and magnetite. Geomicrobiol J 2007a; 24:1-14.

Zegeye A, Huguet L, Abdelmoula M, Carteret C, Mullet M, Jorand F. Biogenic hydroxysulfate green rust, a potential electron acceptor for SRB activity. Geochim Cosmochim Acta 2007b; **71** :5450-62.

Zegeye A., Mustin C., Jorand F. Bacterial and iron oxide aggregates mediate secondary iron mineral formation: green-rust vs magnetite. Geobiology 2010; 8:209-22.

745

750

755

Table 1. Characteristics of the incubation flasks for the biomineralization tests and secondary iron minerals resulting of the DIRB activity at 30°C. ±SD are calculated from duplicate or triplicate incubation flasks or from duplicate analysis on a single sample. Since no detectable Fe^{II} was present in the raw biofilm sample, Fe_{tot} is assumed to correspond to Fe^{III}.

Main electron acceptor	Biofilms as Fe^{III} source (n=2)			Biofilms as inocula (n=3)			Biofilms as inocula and Fe^{III} sources (n=3)
Fe_{tot} (Fe^{III}) mmol l^{-1}	170 mmol l^{-1} (lyophilized biofilm)			60 mmol l^{-1} (synthetic γ-FeOOH)			22, 31 and 57 mmol l^{-1} (freshly sampled biofilm)
Electron donor(s) (mmol l^{-1})	*Formate* 70			*Acetate/formate/lactate* 5/5/2.5			Acetate/formate/lactate 4/4/2 or 15/15/7.5
pH (initial)	*~ 6.5*			*~ 6.5*			*~ 6.5*
Inoculum	*S. putrefaciens*			Biofilm from *Passerelle*[2]	Biofilm aliquot from *Vénus*[2]	Biofilm from *Estuary*[2]	Biofilm suspension (from *Passerelle*)[3]
Initial cell density (cells mL^{-1})	$8.4\ 10^8$	$3.2\ 10^9$	(Control[1])	$\sim 10^8$	$\sim 10^8$	$\sim 10^8$	$2 – 5 \times 10^9$
Ratio cells/Fe^{III} (cells mmol^{-1})	0.5×10^{10}	1.9×10^{10}	/	$\sim 0.2\times10^{10}$	$\sim 0.2\times10^{10}$	$\sim 0.2\times10^{10}$	$\sim 9\times10^{10}$
pH (final)	8.5±0.1	8.5±0.1	nd	nd	nd	nd	8.2±0.1
Max Fe^{II} % Fe^{tot}	51±7%	63±4%	9.4+0.1%	28±1%	39±2%	35.3±0.2%	59±6%
Secondary iron minerals (70 to ~ 800 d)	GR1 M and CMC (traces)	GR1 M and CMC (traces)	Amorphous solids	Amorphous solids with GR like particles	Amorphous solids with GR like particles	GR1 and vivianite	Amorphous solids with GR like particles

[1]no cell amended.
[2]these inocula consisted by suspensions from biofilms or deposits diluted in the estuarine water, 10 % (V/V) of these suspensions were used as inocula.
[3]60 – 90 % (V/V) of a biofilm suspension. nd = not determined.

Table 2. Physico-chemical characteristics of the water phase and of the ferruginous biofilms at the river stations *Passerelle* and *Vénus* (collected in June 2007). DW = dry weight, AFDW = ash free dry weight, nd = not determined.

	Station	
Parameters	*Passerelle*	*Vénus*
Estuarine water[a]		
pH	5.8	5.6
O_2 mg l^{-1} (%)	5.1 (65)	4.5 (58)
E_h mV	243 - 321	
PO_4^{3-} μg l^{-1}	16.5	17.8
NH_4^+ μg l^{-1}	159	152
Fe^{II}_{aq} μg l^{-1}	922 ($\sim$ 16 μmol l^{-1})	536 ($\sim$ 10 μmol l^{-1})
Tp°C	26.8 – 28.3	
Biofilms		
DW (g m^{-2})[b]	30 – 40[b]	nd
AFDW (% DW)	35 ± 4 (n =16)	34 ± 4 (n = 3)
Fe (g g^{-1} DW)[c]	0.37 ± 0.01 (n = 3)	0.20 ± 0.01 (n = 3)
Fe[d]	8 – 13 % *(26 – 38 %)*	nd
O (O_2^-, R-OH, H_2O)[d]	33 – 35 % *(27 – 33 %)*	nd
N (-NH_2, NH_2^+)[d]	2.6 – 2.7 % *(1.9 – 2.2 %)*	nd
C (-C, H ; C-O, H ; C=O)[d]	51 – 54 % *(32 – 38 %)*	nd
S (R-S-, S^{2-}…)[d]	0.17 – 0.18 % *(0.28 – 0.33 %)*	nd
Bacteria (cells g^{-1} DW)	6 ± 3 × 10^{11}	1.3 ± 0.5 × 10^{11}

[a] Data from Dominique (2006)
[b] Estimation based on the measurement of DW accumulated on a nylon rope staying 8 months in the river at the *Passerelle* station.
[c] from ICP-AES analysis.
[d] % of the relative abundance by atoms or by weight % (in brackets) determined by XPS (n=2). See Table SI-1 for raw data.

Figure legends:

Figure 1. Map showing the location of the Petit-Saut dam and the stations *Passerelle*,

5   *Vénus* and *Estuary* (indicated as a white star) along the Sinnamary Estuary in French

Guiana. The semi-circle indicates the location of the dam.

Figure 2. Pictures of the ferruginous biofilms at the *Passerelle* (a, c, d, e, f) or at the

Vénus stations (b). Photography of the biofilms recovering a tube (5 cm in diameter)

10   or leaflets as substrata at *Passerelle* and *Vénus* stations, respectively. Optical

microscopy picture showing bacterial microcolonies (mc) embedded in organic or Fe-

bearing gel like matrix, organic matter appears in blue due to the Azur blue coloration

(c).Transmission electron microscopy showing close interaction between bacteria

and ferruginous material (d), a crumpled paper like Fe-phase (the inset image

15   represents a selected area electron diffraction pattern revealing the solids as

lepidocrocite) (e), and a non-diffracting granular Fe-phase (f).

Figure 3. a) X-ray diffractogram (Co, $\lambda = 0.17902$ nm) and b) Raman spectra of the

lyophilized ferruginous biofilm (*a*), chemically synthesized ferrihydrite-2-lines (*b*) and

20   lepidocrocite (*c*) as references. Si means SiO_2, L means lepidocrocite and F means

ferrihydrite.

Figure 4. Reduction course of the iron oxide constituting the lyophilized biofilm and

inoculated with *Shewanella putrefaciens* cells. The total Fe^{II} consist in both Fe^{2+} in the

25   soluble and solid phases. The anaerobic incubation of the lyophilized biofilm (25 g l^{-1})

1

was done with 70 mmol l^{-1} of formate as the electron donor and with *S. putrefacioens* cells in duplicate at 8.4×10^8 (open triangle) or 3.2×10^9 (close triangle) cells ml^{-1}. No cell was added in the control (open circle).

30   Figure 5. X-ray diffractograms (Co, λ = 0.17902 nm) of the lyophilized biofilm incubated with a resting cell suspension of *Shewanella putrefaciens* (LC, 8.4×10^8 cells ml^{-1} and HC, 3.2×10^9 cells ml^{-1}) or without *Shewanella* (control). All analysis were made after 70 d of incubation time, an additional analysis was made at 800 d with 3.2×10^9 cells ml^{-1}. GR1 means green rust 1; M, means magnetite and CMC

35   means Calcium Magnesium Iron Carbonate.

Figure 6. TEM micrograph (a) and SEM micrograph (b) of GR crystals from incubation of the lyophilized biofilm with *S. putrefaciens* (70 d of incubation time); optical and TEM pictures from incubation of synthetic γ-FeOOH with aliquot from

40   *Estuary* surface sediment (180 d of incubation time) indicating a GR like crystals (arrow) within an aggregate of iron oxides (c) and a GR crystal with its electron diffraction pattern (d); TEM and optical pictures from incubation of fresh biofilms supplemented with electron donor showing solid diffracting as an hexagonal symmetry and GR like particles (arrow) (180 d of incubation time) (e, f).

45

2

Atlantic Ocean

Estuary

Cr. Toussaint

SINNAMARY

Bravo

Pointe Combi

Cr. Saulner

Vénus

Cr. Chapeau

Chapeau

Cr. Verte

Cr. Vénus

Kerenroch

Passerelle

Artificial water falls

Petit Saut

Bagatelle

5 km

54° 53° 52°

Atlantic Ocean

Awala-Yalimapo

Mana

Saint-Laurent

Apatou

Saint-Élie

Petit Saut Reservoir

Sinnamary

Iracoubo

Sinnamary

Kourou

CAYENNE

Rémire-Montjoly

Roura

Kaw

French Guiana

Saint-Georges

Grand-Santi

Papaïchton

Saül

Regina

Ouanary

SURINAM

Maripasoula

Camopi

BRAZIL

60 km

5°

4°

3°

2°

VENEZUELA

FRENCH GUIANA

COL.

PERU

BRAZIL

BOL.

PARAGUAY

CHILE

ARGENTINA

URUGUAY

Atlantic Ocean

Pacific Ocean

Figure 2

a)

b)

c)

mc

10 μm

d)

Fe + O

Bacteria

0.5 μm

e)

Fe + O

0.2 μm

f)

Fe + O

0.2 μm

5

10

15

a)

b)

5

Figure 3.

5

Figure 4.

Fig. 5
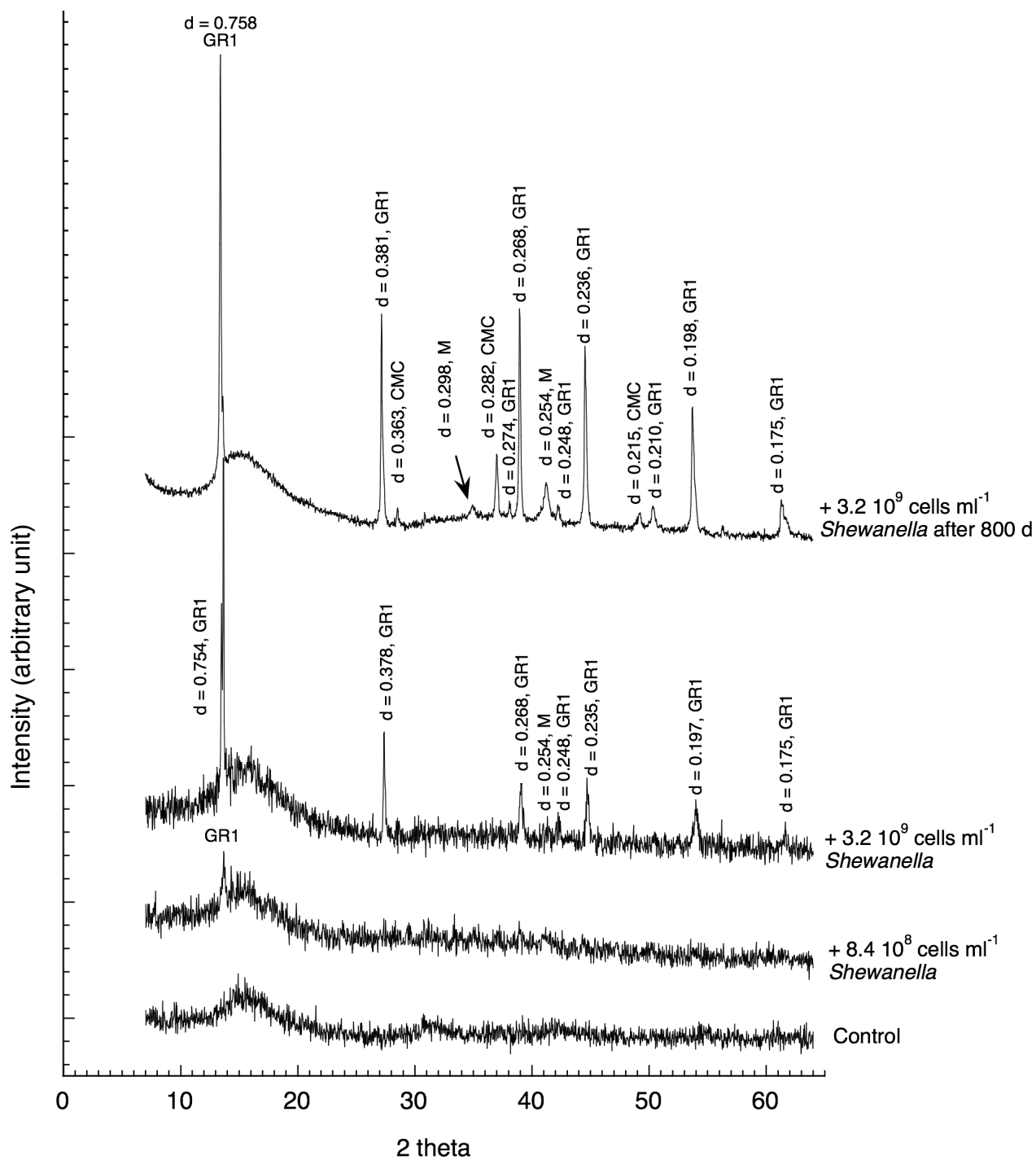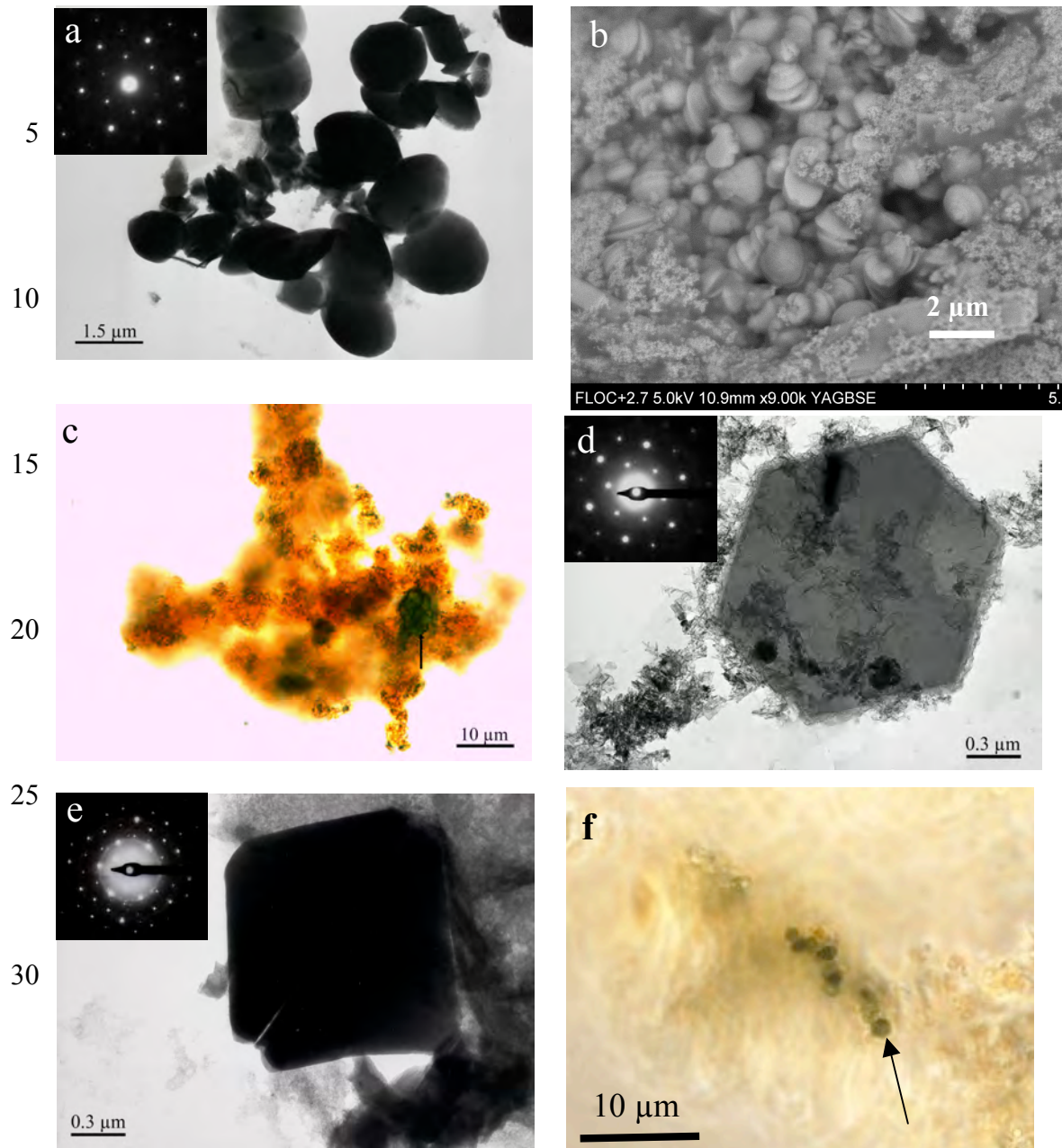
Figure 6.

Supporting information

The formation of green rust induced by tropical river biofilm components

Table SI-1. Quantification report from XPS analysis

Peak	Position BE (eV)	FWHM (eV)	Raw area (cps)	RSF	Atomic conc %	Mass conc. %
Fe_2p	710.788	3.777	14822.1	1.971	8.33	27.13
O_1s	530.888	3.332	23741.1	0.780	35.00	32.65
N_1s	399.588	2.147	1104.9	0.477	2.73	2.23
C_1s	284.588	1.522	12348.2	0.278	53.76	37.66
S_2p	162.988	2.016	91.7	0.668	0.18	0.33

Table SI-2. d_{hkl} parameters of lepidocrocite from literature and from this study.

(*hkl*)	d_{hkl} (nm) from literature		d_{hkl} (nm) from this study	
	Ref [a]	Ref [b]	By electronic diffraction (Fig. 2c)	By XRD (Fig. 3a)
(200)	0.626	0.634	-	0.620 – 0.765
(210)	0.329	0.333	0.331	0.322 – 0.332
(301)	0.247	0.250	0.244	0.243 – 0.256
(111)	0.238	0.236	0.237	0.233 – 0.241
(501)	0.193	0.196	0.195	0.192 – 0.197

[a] Cornell and Schwertmann (1996).
[b] Zegeye *et al.* (2007).

Table SI-3. Mössbauer hyperfine parameters of spectra measured at room temperature of the lyophilized ferruginous biofilms.

	δ (mm s^{-1})	Δ (mm s^{-1})	RA
D_L	0.33	0.55	74 %
D_F	0.34	0.91	26 %

δ = isomer shift taking α-iron as reference at ambient; Δ, quadrupole splitting; RA, relative abundance.
D_L = doublet from lepidocrocite; D_F = doublet from ferrihydrite.

Table SI-4. d_{hkl} parameters of GR1(CO$_3$$^{2-}$) from literature and from this study.

(hkl)	d_{hkl} (nm) from literature			d_{hkl} (nm) from this study (Fig. 5)	
	Ref.[a]	Ref.[b]	Ref.[c]	Electronic diffraction	XRD
(003)	0.7530	0.751	0.755	-	0.752-0.764
(006)	0.3759	0.373	0.381	-	0.378-0.381
(101)	0.2720	0.273	0.274	-	0.274
(012)	0.2668	0.265	0.269 0.267[d]	0.272	0.268
(015)	0.2344	0.233	-	-	0.235-0.236
(018)	0.1967	0.196	0.198	-	0.197-0.198
(0012)	0.1880	0.188	0.190	-	0.188-0.190
(1010)	0.1740	0.173	0.175	-	0.175
(120)	0.1550		0.156[d]	0.158	-

[a] Hansen *et al.* (1989).
[b] Drissi *et al.* (1995).
[c] Jorand *et al.* (2007).
[d] Data from electronic diffraction.

Table SI-5. Mössbauer hyperfine parameters of spectra measured at room temperature after bioreduction of the lyophilised biofilm by *Shewanella putrefaciens*.

	δ (mm s^{-1})	Δ (mm s^{-1})	H (kOe)	RA
D$_1$ (Fe^{II}$_{GR}$)	1.21	1.99		35 %
D$_4$ (Fe^{III}$_{GR}$)	0.34	0.57		25 %
D$_3$ (Fe^{II}$_{CMC}$)	1.12	2.66		13 %
D$_2$ (Fe^{II}$_L$)	0.15	0.47		7 %
S$_1$ (magnetite)	0.28	0	483	6 %
S$_2$ (magnetite)	0.62	0	452	13 %

δ = isomer shift taking α-iron as reference at ambient; Δ, quadrupole splitting; RA, relative abundance; H; hyperfine field. GR = green rust, CMC = Calcium Magnesium Iron Carbonate.

References

Cornell RM, Schwertmann U (1996) The iron oxides: structure, properties, reactions, occurrences and uses, VCH, Weinheim, Germany.

Hansen HCB (1989) Composition, stabilization, and light absorption of Fe(II)Fe(III) hydroxy carbonate Green Rust. *Clay Minerals* **24**, 663–669.

Drissi H, Refait P, Abdelmoula M, Génin JMR (1995) The preparation and thermodynamic properties of Fe(II)-Fe(III) hydroxide-carbonate (Green Rust 1); Pourbaix diagram of iron in carbonate-containing aqueous media. *Corrosion Sciences* **37**, 2025–2041.

Jorand F, Zegeye A, Landry F, Ruby C (2007) Reduction of ferric green rust by *Shewanella putrefaciens*. *Letters in Applied Microbiology* **45**, 515 – 521.

Supporting information

The formation of green rust induced by tropical river biofilm components

5

SI Figure Caption:

Fig. SI-1. EDX analysis of the second phase analyzed from the biofilm (from Fig. 2f).

10

Fig. SI-2. Mössbauer spectra measured at ambient temperature of the lyophilized biofilm. See Table SI-2 for indication.

Fig. SI-3. Mössbauer spectra measured at ambient temperature of the lyophilised biofilm after bioreduction by *Shewanella putrefaciens*. See Table SI-4 for indication.

15

Fig. SI-4. X-ray diffractogram (Co, l = 0.17902 nm) of the solids from incubation of synthetic γ-FeOOH with aliquot from *Estuary* surface sediment ($\sim$ 3 years of incubation time) indicating green rust (GR1) and vivianite (V).

20

Fig. SI-5. Images from fresh ferruginous biofilms (*Passerelle* site) showing elements (arrows) suggesting twisted like structure from *Gallionella* sp., by optical microscopy (a) and by scanning electronic microscopy (b).

Fig. SI-1
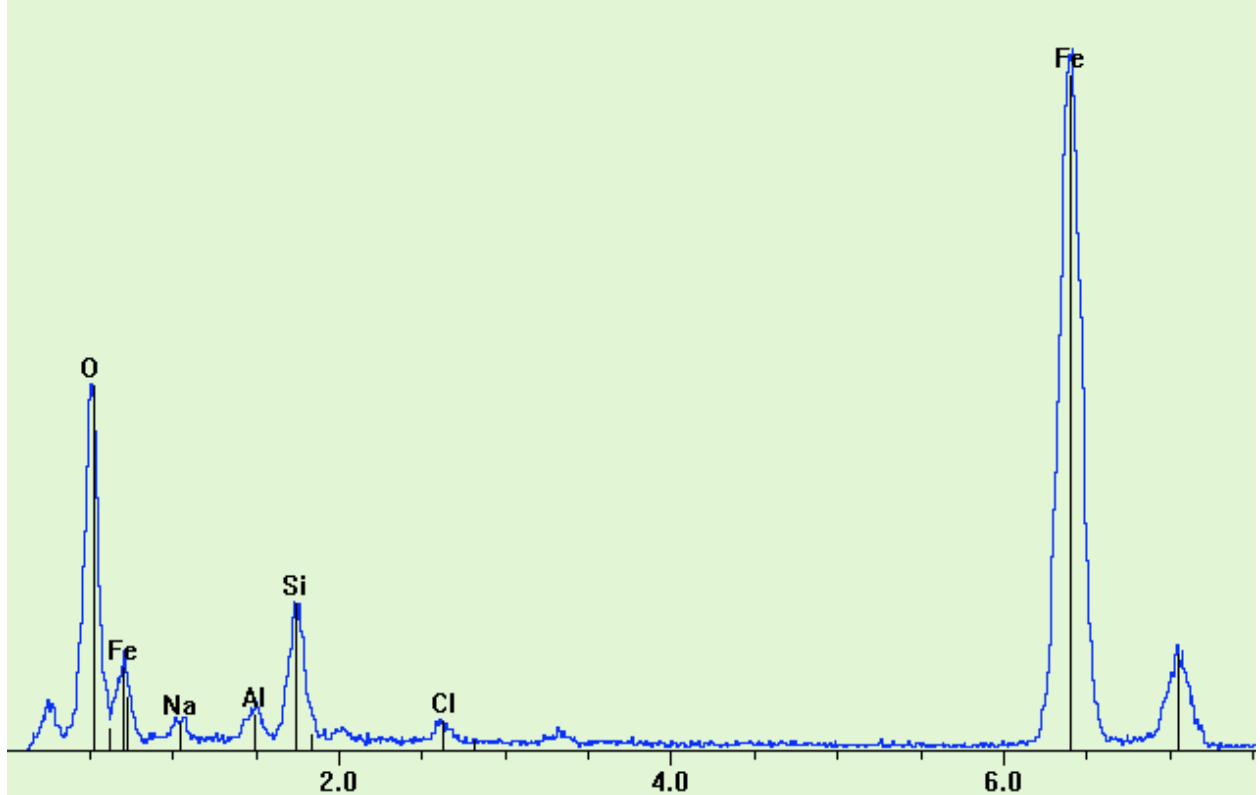
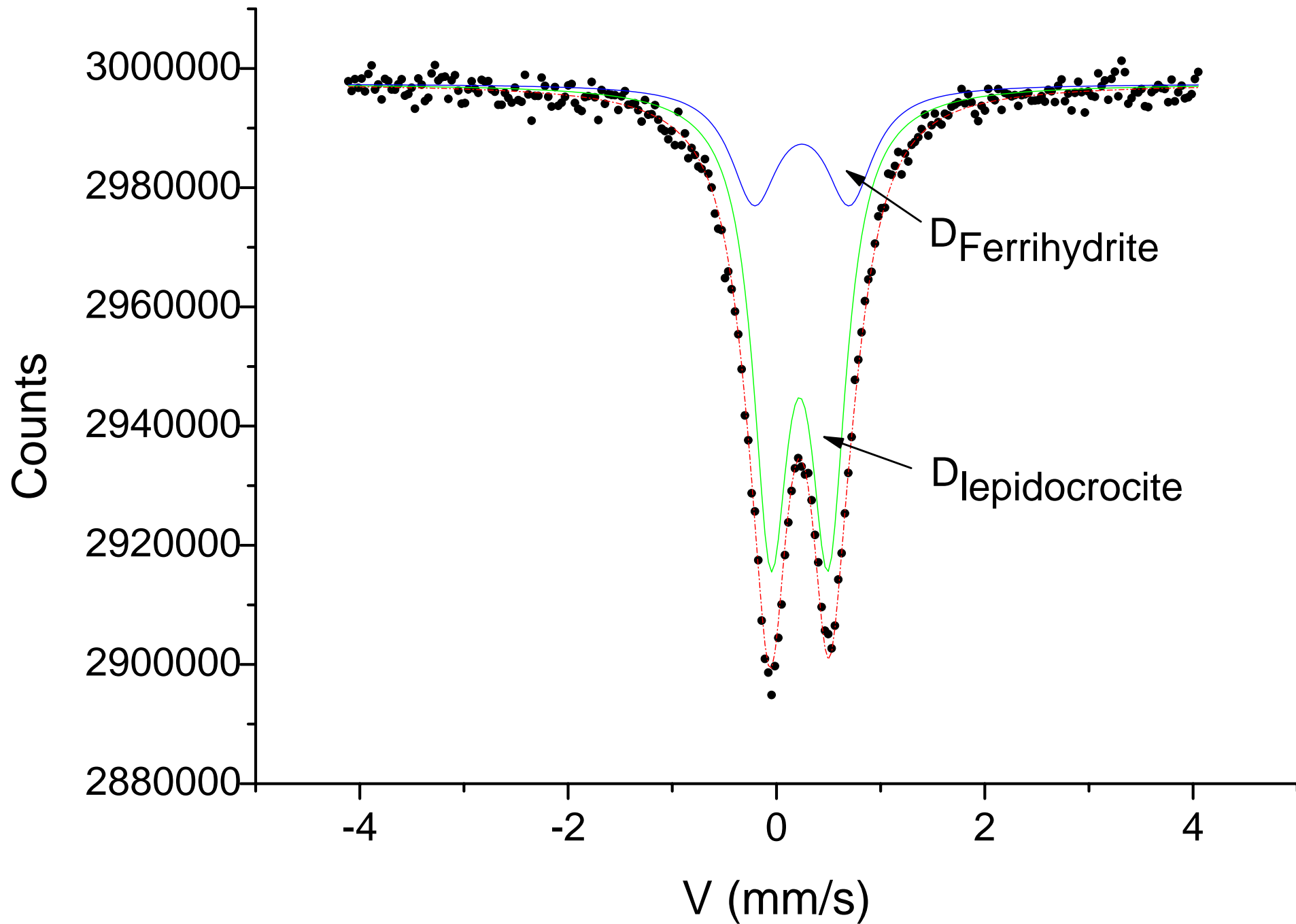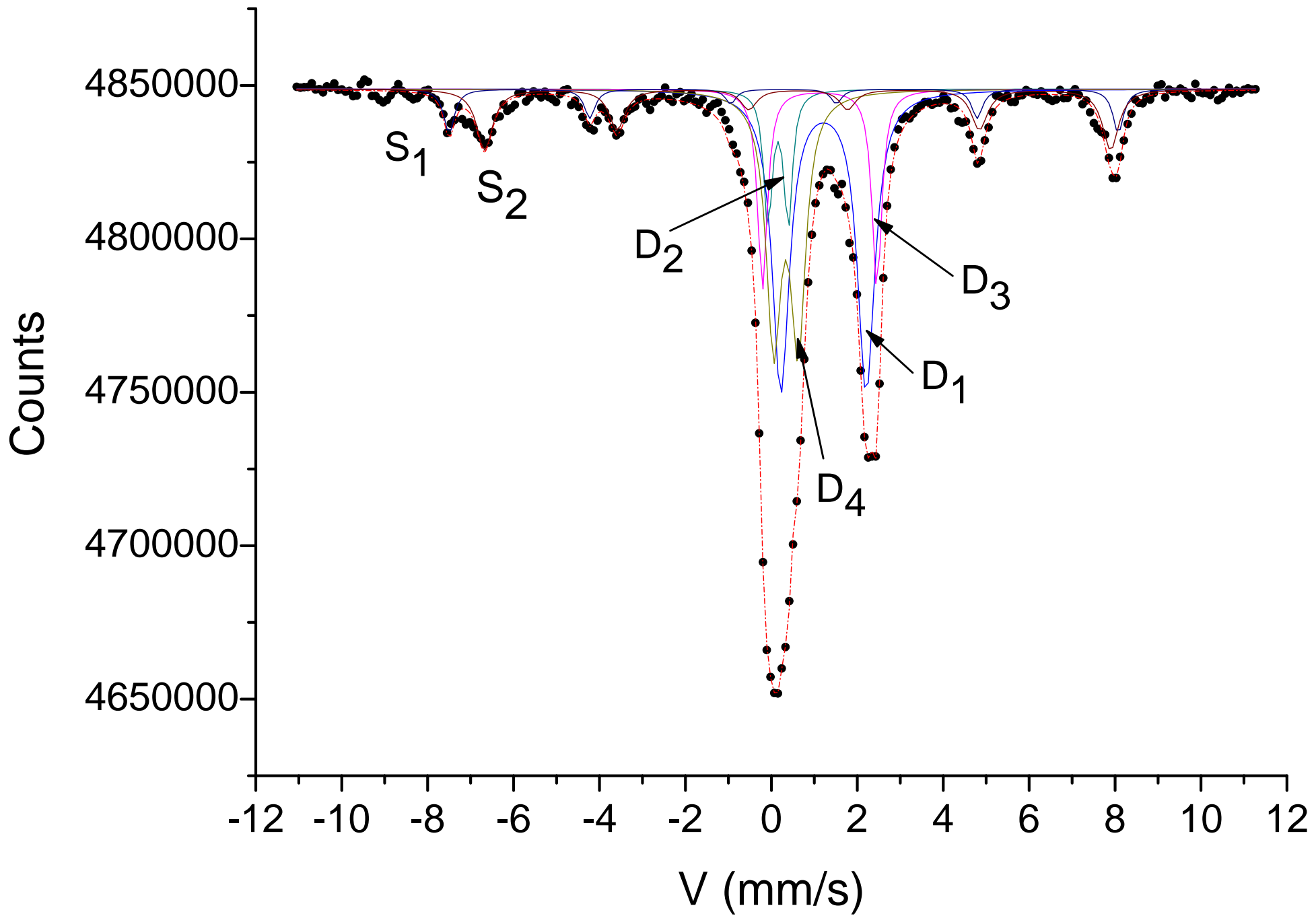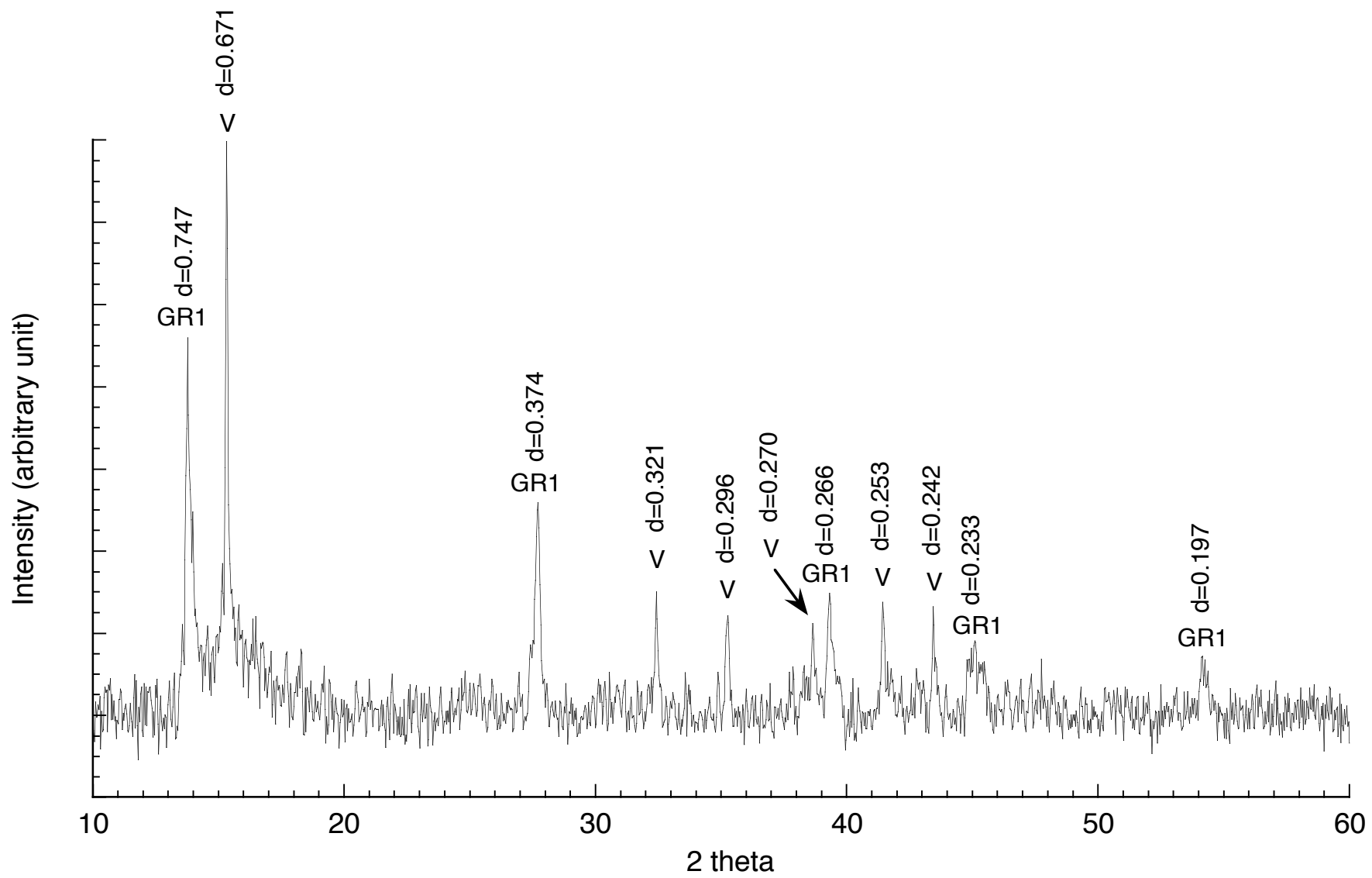| Element	Line	keV	CL Ratio	Wt%	At%
O	KA1	0.523	2.3200	31.16	57.73
Na	KA1	1.041	1.7000	2.58	3.33
Cl	KA1	2.622	1.3000	1.25	1.05
Fe	KA1	6.403	1.4800	58.65	31.13
Si	KA1	1.740	1.0000	5.07	5.35
Al	KA1	1.487	1.0400	1.28	1.41
Total			**0.0000**	**100.00**	**100.00**

Fig. SI-2

Fig. SI-3

Figure SI-4

5

Fig. SI-5